Available online at https://link.springer.com/journal/42241
http://www.jhydrodynamics.com
Journal of Hydrodynamics, 2021, 33(6): 1148-1161
https://doi.org/10.1007/s42241-022-0112-6

Wake flow and vortex structures behind emergent vegetation patches elongated in the longitudinal direction *

Zi-jian Yu[1, 2], Yu-qi Shan[1, 3], Chao Liu[1], Xing-nian Liu[1]
1. *State Key Laboratory of Hydraulics and Mountain River Engineering, College of Water Resource and Hydropower, Sichuan University, Chengdu 610065, China*
2. *Department of Civil and Environmental Engineering, University of Alberta, Edmonton, Canada*
3. *Institute for Disaster Management and Reconstruction, Sichuan University, Chengdu 610065, China*

(Received April 9, 2021, Revised June 2, 2021, Accepted June 10, 2021, Published online January 7, 2022)

Abstract: In natural rivers, patches of vegetation generally expand over their steady wake region in the streamwise direction, forming elongated patches with length (L) greater than their width (b). This paper studies how the wake flows and the vortices develop as the emergent patches expand their length in the streamwise direction. The patches are modeled with the same width but different lengths in laboratory experiments. Behind the patches, the steady wake region (L_w) is not related to the width-related flow blockage $(C_d ab)$, where C_d is the drag coefficient, a is the vegetation density. Instead, L_w is related to the length-related flow blockage $(C_d aL)$. On this basis, a model is proposed for predicting L_w, which is in good agreement with the measurements. As a patch becomes denser and/or longer (as $C_d aL$ increases), the steady wake region becomes shorter (L_w decreases), and vortices are observed closer to the patch trailing edge, producing a turbulence of a greater magnitude beyond L_w. When the flow blockage increases to the limit $(C_d aL > 8)$, the Karman vortices are observed directly behind the porous patches. These results can be used to explain the longitudinal elongation of the vegetation patches in the field.

Key words: Velocity profiles, turbulent kinetic energy, wakes, vortex streets, vegetation patch

Introduction

The vegetation patches with finite lengths and widths are widely found in natural rivers and intertidal regions[1]. Typical vegetation patches (e.g., *Callitriche platycarpa* patches) expand in the flow direction, with the patch width D, length L often ranging from 0.2 m to 5.0 m[1-2]. Previous studies confirmed that the vegetation patches grow along the riverbank and may affect the landscape of rivers by altering the flow structures within, laterally beside and behind the patches[1]. Within a patch, the vegetation drag reduces the flow velocities[3], which suppresses the resuspension of fine sediment[4]. Suspended sediment with nutrients attached tends to deposit in the vegetated regions, to promote the vegetation growth, resulting in a denser patch[5]. The flow entering the patch is deflected to the adjacent bare channel, producing the local flow acceleration and the bed erosion, which restrict the patch lateral extension[6]. In the patch wake, a low-velocity wake region forms and helps the sediment deposition, which may facilitate the longitudinal extension of the patch[7]. Overall, due to the altered flow structures and the sediment deposition, a vegetation patch would generally become denser and/or extend in the longitudinal direction.

To explore the interaction between the model patch, the flows and the bed morphology, laboratory studies were conducted to measure the flow field and the geomorphology in detail within and around the model patches[4, 8-13]. When the flow encounters the leading edge of an emergent vegetation patch, a portion of the flow is deflected out of the patch, while the rest goes through the patch. Within the patch, the distance between the patch leading edge and the point inside the patch, at which the flow velocity is either constant or at its minimum, is defined as the interior

* Projects supported by the National Natural Science Foundation of China (52022063, 52179074 and U2040219).
Biography: Zi-jian Yu (1996-), Male, Ph. D. Candidate,
E-mail: spencer6@ualberta.ca
Corresponding author: Chao Liu,
E-mail: chaoliu@scu.edu.cn

flow adjustment distance, L_I, which can be predicted as[3]

$$L_I = (5.5 \pm 0.4)\sqrt{\left(\frac{2}{C_d a}\right)^2 + b^2} \quad (1)$$

Zong and Nepf[14] reported that the exit velocity from the patch, can delay the occurrence of the von Karman vortex street behind the patch and that a steady wake region with a length L_w is formed between the trailing edge of the patch and the onset of the vortex. For an emergent circular patch, Zong and Nepf[14] suggested that L_w, normalized by the patch width, b, is related to two shear layers formed behind the patch

$$\frac{L_w}{b} = \frac{1}{4S_1}\frac{U_{\text{bare}} + U_e}{U_{\text{bare}} - U_e} \approx \frac{1}{4S_1}\frac{1 + U_e / U_\infty}{1 - U_e / U_\infty} \quad (2)$$

where S_1 is a scale parameter, U_{bare} is the velocity in the bare channel laterally beside the wake, U_e is the exit velocity at the trailing edge of a patch and U_∞ is the mean channel velocity. Zong and Nepf[14] suggested that $S_1 = 0.10 \pm 0.02$ for emergent patches with $a = 6\ \text{m}^{-1}$ - $29\ \text{m}^{-1}$ under the flow conditions of $U_\infty = 0.10\ \text{m/s}$, $H = 0.13\ \text{m}$. The patch width is generally much smaller than the channel width (e.g., $b/B = 0.13$ in this study), thus, $U_{\text{bare}} \approx U_\infty$ is a reasonable assumption (see Table 1), yielding the last term of Eq. (2), i.e., $(1/4S_1)[(1 + U_e/U_\infty)/(1 - U_e/U_\infty)]$.

The suspended sediment attached with organic matter and nutrients is preferentially deposited in the steady wake region, in which the velocities and the turbulent kinetic energy (TKE) are diminished[15]. Previous studies focused either on the wake flows behind circular patches[16-17] or on the longitudinal evolution of the flows inside rectangular patches with the same width but different lengths[3]. In some studies[15-17], the dimensionless parameter $C_a ab$ was used to establish the relationship with the steady wake region length, L_w, normalized by the patch width, b, where $C_a ab$ represents the flow blockage of a patch in the lateral direction. However, in these studies, the patch elongation in the streamwise direction is not duly considered. In natural rivers, the vegetation patches generally expand in the streamwise direction, however, the above studies did not focus on the evolution of flows and vortices behind such patches extending in the streamwise direction. As a consequence, the elongation of the patches in the field has not been explained from a hydrodynamic viewpoint. Thus, clarifying these aspects is one goal of this study.

The velocity distributions inside and outside the emergent circular patches of the model vegetation were studied in numerical simulations[18], but the wake flow behind the elongated patches was not duly considered. Recently, the velocity distributions upstream and inside an emergent rectangular model patch were predicted based on analytical models[19-20], but these models cannot be used to predict the velocity distribution in the wake. Accordingly, there were no numerical or analytical models available to predict the length of the wake region. This paper proposes a method to predict the length of the steady wake region behind an elongated patch and to further explore the expansion pattern of the vegetation patches.

1. Method

Experiments are conducted in a 20.0 m long, 1.5 m wide and 0.6 m high straight Plexiglas flume with a bed slope of 0.1%. The flow discharge ($Q = 0.031\ \text{m}^3/\text{s}$), the flow depth ($H = 0.15\ \text{m}$) are the same in all cases. The water passes through a flow straightener to produce a laterally uniform velocity distribution at the entrance of the test section. The mean channel velocity is $U_\infty = 0.10\ \text{m/s}$, which is within the range of 0.10 m/s to 0.25 m/s, as measured in wetlands and lowland rivers[4, 21]. The slope of the water surface is made the same as the bed slope by adjusting the tailgate. The flow is turbulent in all cases with $Re(=U_\infty R/\nu) = 16\,914$, in which R is the hydraulic radius, ν is the kinematic viscosity. The flow is in the subcritical state with $Fr(=U/\sqrt{gh}) = 0.11$, where g is the local gravity acceleration. The bed friction coefficient of the baseboards, $C_f = 0.006$, as was determined by Liu and Shan[3] under similar flow conditions ($U_\infty = 0.18$ m/s, $H = 0.18$ m). The bed roughness may depress the formation of the Karman vortices; thus, the stability parameter $S_w(=C_f b/h)$ was calculated to examine the impact of the bed roughness on the vortex formation, in which b is the width of a model patch. In this study, $S_w(=0.01)$ is much smaller than the critical value (= 0.2, for a solid cylinder with a diameter of 0.4 m), indicating that the baseboards will not influence the formation of the Karman vortices behind patches. In this study, the drag coefficient, $C_d = 1$, is taken for simplicity.

Rigid circular cylinders fixed to the baseboards in a staggered arrangement are used to simulate the rigid vegetation (Fig. 1). The diameter of the individual cylinder is $d = 0.008$ m. The cylinder length

(= 0.3 m) is greater than the flow depth (0.15 m), thus, the model patches are emerged in all cases. The vegetation density is set as $n = 1\ 300\ \mathrm{m}^{-2}$, $3800\ \mathrm{m}^{-2}$, to match the range of densities, i.e., $n = 400\ \mathrm{m}^{-2}$ - $3\ 700\ \mathrm{m}^{-2}$, for cordgrass (e.g., *S. alterniflora*). The frontal area per patch volume is $a\,(= nd) = 10\ \mathrm{m}^{-1}$, $30\ \mathrm{m}^{-1}$. To investigate the impact of the patch length on the wake structure, the patch width $b = 0.2$ m is chosen in all cases, but with a varied patch length, L. Specifically, five patch lengths ($L = 0.2$ m, 0.4 m, 0.6 m, 0.8 m and 1.0 m) are chosen for $a = 10\ \mathrm{m}^{-1}$, corresponding to $L/b = 1.0$, 2.0, 3.0, 4.0 and 5.0, respectively. Six patch lengths ($L = 0.2$ m, 0.4 m, 0.5 m, 0.6 m, 0.8 m and 1.0 m) are chosen for $a = 30\ \mathrm{m}^{-1}$, corresponding to $L/b = 1.0$, 2.0, 2.5, 3.0, 4.0 and 5.0, respectively. The experimental parameters are summarized in Table 1.

1.1 *Velocity measurements*

The longitudinal, lateral, and vertical directions are chosen as x, y and z, respectively. $x = 0$ indicates the upstream edge of a model patch, $y = 0$ indicates the centerline of the flume and the patch and $z = 0$ indicates the surface of the channel bed (Fig. 2). The instantaneous streamwise velocity $u(t)$, the lateral velocity $v(t)$ and the vertical velocity $w(t)$ are measured with a Nortek acoustic Doppler velocimeter (ADV) equipped with a downward-looking probe. The ADV is installed on a measurement bridge, which could move in the x, y and z directions. The preliminary experiment confirms that behind a patch, the time-averaged velocities and TKE become constant when the recording period of the ADV is equal to or greater than 300 s with a recording frequency of 50 Hz. Hence, at each position behind a patch, it is reasonable to set the recording period and frequency as 300 s and 50 Hz, respectively. The raw data are despiked using the method proposed by Goring and Nikora[22]. The instantaneous velocities ($u(t)$, $v(t)$ and $w(t)$) with correlations less than 85% and a signal-to-noise ratio smaller than 25 dB are removed. A MATLAB code is used to extract the time-averaged velocities (u, v and w) and the fluctuation components (u', v' and w'). The TKE measured at each position is defined as $\mathrm{TKE} = (\overline{u'^2} + \overline{v'^2} + \overline{w'^2})/2$. The measurement noise in the velocity (= 0.001 m/s) and the TKE (= 2.1150×10^{-6} $\mathrm{m}^2/\mathrm{s}^2$) is determined in the flume without upstream or drainage velocities (i.e., in still water). Velocity is measured once at each position to obtain the longitudinal profiles of the streamwise velocities. Measurements are repeated twice at selected positions (e.g., $x \approx L$) to obtain the uncertainty margin for

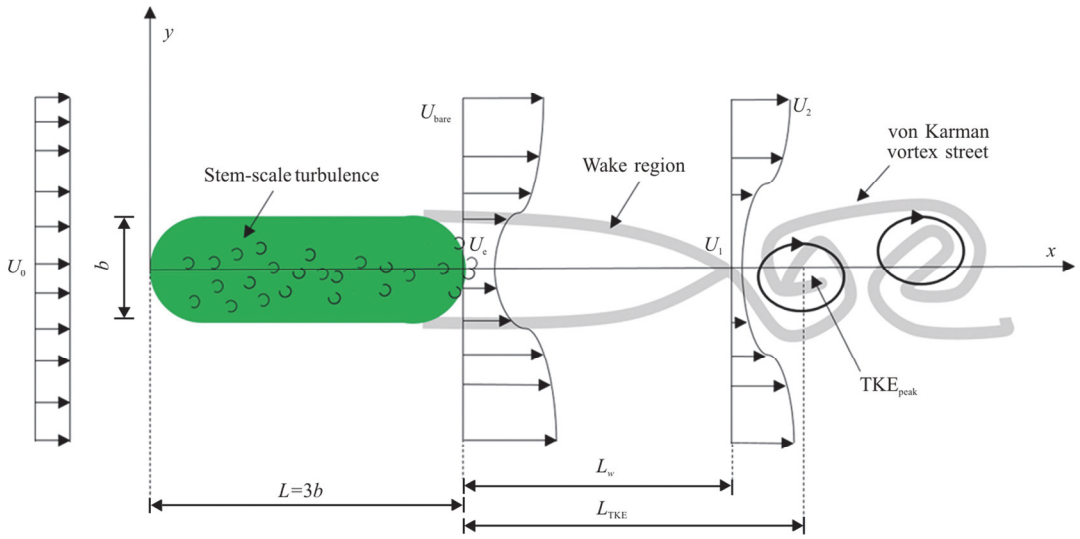

Fig. 1 (Color online) Schematic views of an extended patch of emergent vegetation (with case B4 as an example, $a = 30\ \mathrm{m}^{-1}$, $L = 0.6$ m), shown by the green elongated capsule of width $b\,(= 0.2\ \mathrm{m})$. The thick gray lines at the outer edges of the patch reveal the evolution of the wake. The velocity of the flow from the patch (U_e) is measured at the centerline of the patch and at the position closest to the patch trailing edge, which is reduced relative to the upstream velocity (U_∞) and the velocity in the bare area (U_{bare}). The velocity (U_1) decreases further at the onset of the von Karman vortex street (end of the steady wake, $x = L + L_w$). The patch-scale turbulence (black circles with arrows) peaks are at the position of $x = L + L_{\mathrm{TKE}}$

Table 1 Experimental parameters

Case	L /m	$C_d aL$	U_{bare} /m·s^{-1}	U_1 /m·s^{-1}	U_2 /m·s^{-1}	TKE_{peak} /m^2·s^{-2}	L_{TKE} /m	L_I /m
A1	0.2	2	0.132±0.005	0.029±0.001	0.143	0.08±0.01	2.40±0.20	1.17±0.09
A2	0.4	4	0.134±0.006	0.026±0.001	0.144	0.11±0.02	1.10±0.10	1.17±0.09
A3	0.6	6	0.136±0.008	0.009±0.002	0.149	0.16±0.01	0.80±0.10	1.17±0.09
A4	0.8	8	0.138±0.011	–0.008±0.002	0.149	0.17±0.01	0.65±0.05	1.17±0.09
A5	1.0	10	0.137±0.013	–0.015±0.001	0.150	0.19±0.03	0.40±0.05	1.17±0.09
B1	0.2	6	0.130±0.009	–0.012±0.001	0.149	0.23±0.03	0.80±0.10	0.63±0.05
B2	0.4	12	0.131±0.011	–0.011±0.001	0.150	0.36±0.03	0.55±0.05	0.63±0.05
B3	0.5	15	0.129±0.017	–0.018±0.001	0.150	0.32±0.07	0.50±0.05	0.63±0.05
B4	0.6	18	0.131±0.017	–0.015±0.001	0.150	0.37±0.09	0.45±0.05	0.63±0.05
B5	0.8	24	0.138±0.015	–0.009±0.001	0.149	0.39±0.12	0.40±0.05	0.63±0.05
B6	1.0	30	0.136±0.009	–0.011±0.002	0.150	0.39±0.12	0.20±0.05	0.63±0.05

Note: L is the patch length, U_{bare} is the velocity in the bare channel laterally beside the wake, U_1 is the centerline velocity at the end of the wake region, U_2 is the mean velocity outside the vegetated area calculated with U_1 based on the flow continuity, TKE_{peak} is the maximum magnitude of the turbulent kinetic energy behind the patch and L_{TKE} is the distance from the patch trailing edge to the beginning of the von Karman vortices (see Fig. 1(b)) and L_I is the interior flow adjustment distance inside a patch.

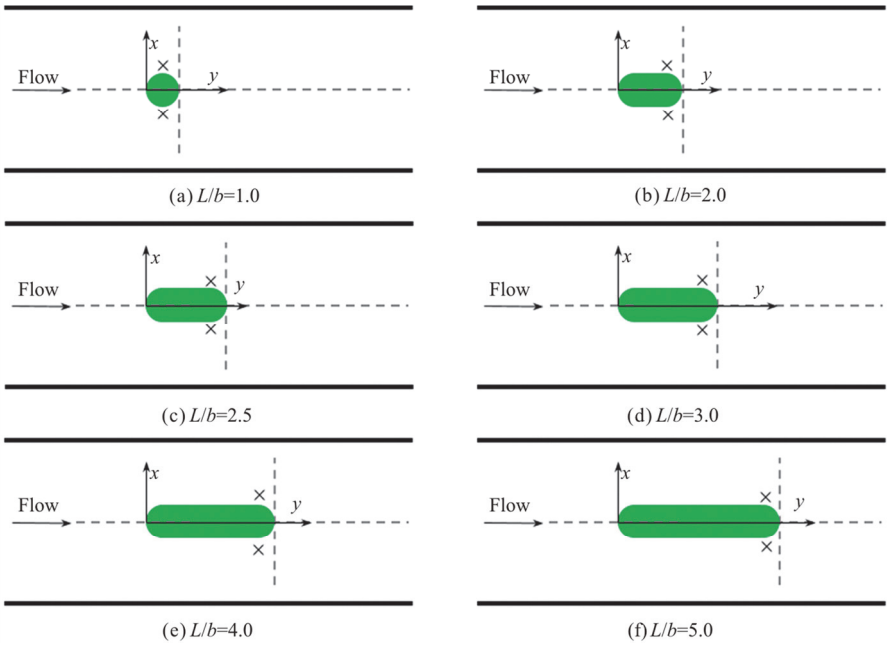

Fig. 2 (Color online) Model patches of the vegetation, measurement positions and dyed injection points. L and b are the patch length and width, respectively. Measurement transects in the longitudinal and lateral directions are denoted by dashed lines. In all cases, a longitudinal transect is set at the centerline of the channel and the patches. Seven lateral transects are arranged for the initial circular patch in (a). Three lateral transects are arranged for the other elongated patches. The green region indicates a model patch. The dyed injection points are denoted by "X" in each subplot

velocities. The lateral velocity spectrum S_{vv} is obtained using the continuous wavelet transform with a time step of 1/50 s. The velocity spectra are used to determine whether the Karman vortices are sufficiently strong to stand out relative to the turbulence within the channel.

The velocity measurement transects are represented by dashed lines in Fig. 2. The longitudinal distributions $(y = 0)$. The lateral distributions of the velocities are measured at the transects at the trailing edges of the initial circular patch (Fig. 2(a)) and the elongated patches (Figs. 2(b)-2(f)). At each position,

the velocities are measured at the mid-depth ($z = h/2$). For the emergent patches, the flow in the channel with an emergent patch varies mainly in the x- and y-directions, thus, the mid-depth velocities, U, are representative, with a difference from the depth-averaged velocities less than 6%. This fact is confirmed by Liu and Shan[3]. Behind a patch, the length of the steady wake region, L_w, is the distance between the patch trailing edge of the patch and the position of the smallest velocity downstream the patch, over which the velocities are smaller than the exit velocity (U_e). U_e is measured at the centerline of the patch and at the position closest to the patch trailing edge. L_w is estimated from the measured longitudinal profile of velocities. The velocities begin to increase at $x = L_w$ due to the flow mixing. If the shear layer is sufficiently strong, the Karman vortices are observed behind the patches.

1.2 *Tracer experiments*

Two needles fixed at the outermost sides of the patches are used to continuously inject the fluorescein to detect the development of the vortices behind the patches. The tracer experiment and the velocity measurements are conducted separately to avoid the mutual influence. The dyed injection positions are denoted by "X" in each subplot in Fig. 2. A Nikon D7200 camera is placed above the wake region behind each patch to capture the motion of the fluorescein and further determine the length of the steady wake region. Specifically, two dyed streams are formed on two sides of each patch, which then merged due to the formation of the von Karman vortex street. The length of the steady wake region, $L_{w(\mathrm{dye})}$, indicated by the visualization is defined as the distance between the trailing edge of the patch and the point at which the two dyed streams are merged (the onset of the Karman vortex). Because the period of the vortex is approximately 1 s-12 s under similar flow conditions, i.e., $H = 0.13\,\mathrm{m} - 0.20\,\mathrm{m}$, $U_0 = 0.09\,\mathrm{m/s} - 0.24\,\mathrm{m/s}$ [14-15], the period of the video recording in this study is 30 s to 40 s at the speed of 24 frames per second, which is sufficient to cover several vortex cycles. In each case, the video contains 720 to 960 images.

Adobe Photoshop CS6 is used to superimpose the black grids in each image accounting for the parallax. At the centerline of the flume and the patch, the distance between the trailing edge of the patch and the most upstream position of the dyed stream is defined as the steady wake region, the length of which is denoted $L_{w(\mathrm{dye})}$. In each case, 20 images are processed separately to obtain $L_{w(\mathrm{dye})}$. The mean value of $L_{w(\mathrm{dye})}$ and its standard deviation (SD) are calculated. Case A3 is taken as an example to show the determination of $L_{w(\mathrm{dye})}$ and SD (see Figure S1 in the supporting information).

2. Results

2.1 *Flow velocity*

For model patches with different lengths, L, normalized by the patch width b (different L/b), the velocities in the wake of a patch U, normalized by the channel-averaged velocity, U_∞, are plotted in Fig. 3, in which only patches with $L/b = 1$, 3 and 5 are shown for clarity. Behind small-density patches ($a = 10\ \mathrm{m}^{-1}$), the length of the steady wake region behind the patch, L_w, decreases with the increase of the patch length, L. Specifically, the shortest patch ($L/b = 1$, Fig. 3(a)) has the longest steady wake ($L_w = 1.10 \pm 0.20$ m, black squares), over which U/U_∞ ranges between 0.2, 0.3. As the patch length, L, is increased to $3b$ (red circles), the length of the steady wake region is decreased to $L_w = 0.50 \pm 0.05$ m, and the velocities in the region are decreased ($U/U_\infty = 0.07 - 0.15$). The longest patch ($L/b = 5.0$, blue triangles) produces a vague steady wake region with a negligible length, i.e., $L_w = 0.05 \pm 0.05$ m, in which negative velocities are observed due to the flow recirculation. Similarly, for high-density patches ($a = 30\ \mathrm{m}^{-1}$), the length of the steady wake region is also decreased as the patch length is increased. Negative velocities are observed in the wakes of three patches ($L/b = 1.0$, 3.0 and 5.0, Fig. 3(b)) because the recirculation flow occurs behind the three patches. A distinct steady wake region is observed behind the shortest patch ($L_w = 0.60 \pm 0.10$ m, black squares). For two longer patches ($L/b = 3.0$ (red circles), 5.0 (blue triangles)), the length of the steady wake regions ($L_w = 0.10 \pm 0.05$ m, 0.05 ± 0.05 m, respectively) is significantly reduced. Based on the above analysis, it is shown that a longer or denser patch will produce a shorter wake region relative to the initial circular patch. It is noted that this statement is valid for patches shorter than the interior flow adjustment distance, L_I, because the flow in the patches is not fully developed. If a patch is longer than L_I, the flow at the place $L > L_I$ is fully developed, and the exit velocity is constant; thus, the length of the wake region does not change.

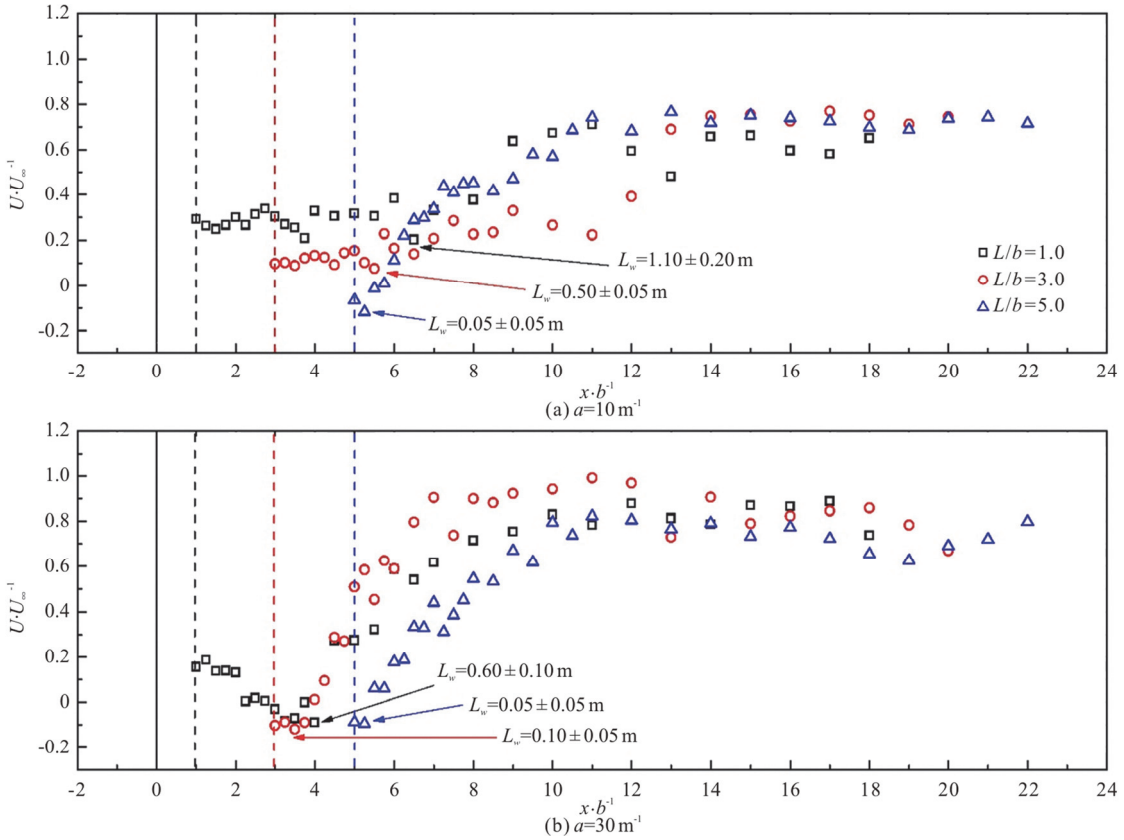

Fig. 3 (Color online) Velocity distributions behind patches for two densities. Velocities, U, are measured at the mid-depth $(z = H/2)$ and the centerline of the patch wakes $(y = 0\ \text{m})$. The two plots include data only in three cases, with the patch lengths, L, normalized by the patch width, b, for clarity (i.e., $L/b = 1.0$, 3.0 and 5.0). U_∞ is the mean channel velocity. The vertical solid lines at $x/b = 0$ indicate the upstream edge of each patch. The black, red and blue vertical dashed lines indicate the trailing edge of the patch for $L/b = 1.0$, 3.0 and 5.0, respectively. The length of the wake region, L_w, is denoted as in the two subplots

For emergent patches, U_e/U_∞ is related to the patch length, L (normalized by the patch width b), and the density, a. When $a = 10\ \text{m}^{-1}$, U_e/U_∞ decreases from 0.3 to –0.1 as the patch length, L/b, increases from 1.0 to 5.0 (black squares, Fig. 4(a)). This is because the length of five patches $(L = 0.2\ \text{m}\text{-}1.0\ \text{m})$ is shorter than the interior flow adjustment distance $(L_I = 1.17 \pm 0.09\ \text{m})$. The flow inside the patch is not fully developed, and the exit velocity decreases as the patch length increases. For a higher density $(a = 30\ \text{m}^{-1})$, U_e/U_∞ decreases from 0.15 to –0.10 as L/b increases from 1.0 to 3.0 because the length of three patches $(L = 0.2\ \text{m}\text{-}0.5\ \text{m})$ is shorter than $L_I = 0.63 \pm 0.05\ \text{m}$. In other three patches $(L = 0.6\ \text{m}\text{-}1.0\ \text{m})$, which are longer than or equal to L_I, the flow at the place $x > L_I$ is fully developed; thus, U_e/U_∞ remains constant for $L/b \geq 3.0$ (red circles). To examine the influence of both the patch length, L, and the density, a, on U_e, the dimensionless parameter $C_d aL$ is defined to represent the flow blockage of a patch associated with the steady wake region in the longitudinal direction. U_e/U_∞ is a function of $C_d aL$ (Fig. 4(b)). That is, U_e/U_∞ decreases as $C_d aL$ increases from $C_d aL = 0\text{-}8$, and when $C_d aL > 8$, U_e/U_∞ becomes constant. Note that U_e/U_∞ decreases to negative values for patches with $C_d aL > 8$, for which recirculating flows occur behind those patches.

With respect to another dimensionless parameter $C_d ab$ used in previous studies[15-16], for the elongated patches, L_w/b does not depend on $C_d ab$ (Fig. 5(a)). The patch length, L, and the vegetation density, a, both influence U_e and should also influence L_w. L_w/b should depend on the dimensionless parameter $C_d aL$ but not on $C_d ab$. As expected, L_w/b decreases as $C_d aL$ increases (Fig. 5(b)).

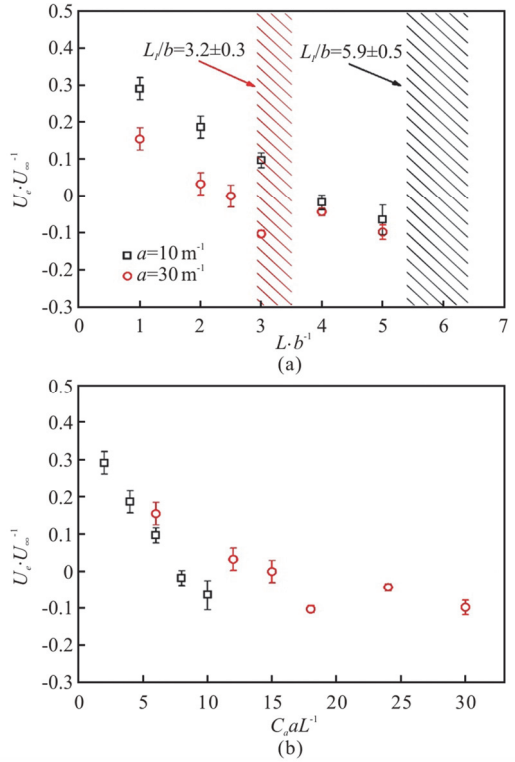

Fig. 4 (Color online) Behind patches with two densities (a = 10 m^{-1}, 30 m^{-1}), the exit velocity, U_e, normalized by the channel average velocity, U_∞, varies with (a) the patch length, L, normalized by the patch width, b. L_I is the interior flow adjustment distance, estimated by Eq. (1). The red and black shaded bars represent the values of $L_I/b(=3.2\pm0.3, 5.9\pm0.5)$ for patches with different densities, $a(=30\ \text{m}^{-1}, 10\ \text{m}^{-1})$, respectively. The width of the bar indicates the uncertainty margin. (b) The nondimensional parameter $C_d aL$ indicates the flow blockage of a patch associated with the wake region in the longitudinal direction

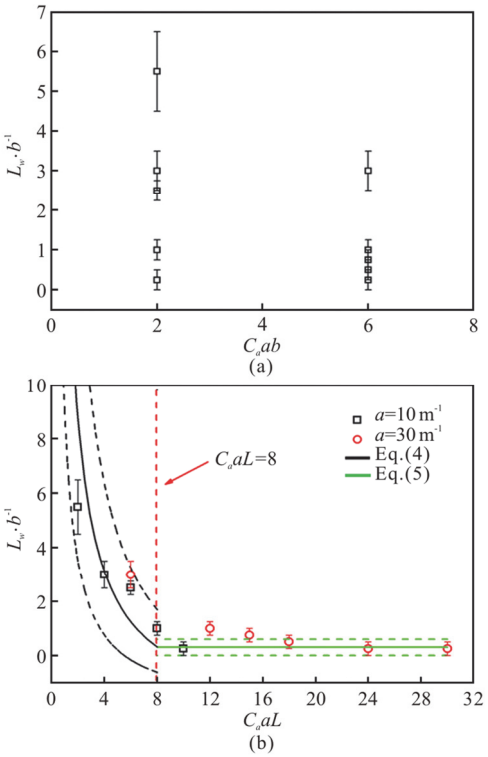

Fig. 5 (Color online) (a) Wake region length, L_w, normalized by the patch width, b, against the nondimensional parameter $C_d ab$, which indicates the flow blockage of a patch in the lateral direction. L_w/b does not depend on $C_d ab$. (b) Relationship between L_w/b, $C_d aL$. $C_d aL$ is a nondimensional parameter indicating the flow blockage of a patch in the longitudinal direction. L_w/b decreases as $C_d aL$ increases for both densities (a = 10 m^{-1}, 30 m^{-1}). The red vertical dashed line indicates $C_d aL = 8$. The black and green dashed lines indicate the margins of uncertainties for the two equations

Next, we discuss how to estimate the length of the steady wake region, L_w, behind elongated patches. Eq. (2) is used to estimate L_w. In this study, the patches ($a = 10\ \text{m}^{-1}$ - $30\ \text{m}^{-1}$) and the flow conditions ($U_\infty = 0.13\ \text{m/s}$, $H = 0.15\ \text{m}$) are similar to those in the study of Zong and Nepf[14], thus, the value of $S_1(=0.10\pm0.02)$ is taken. To predict L_w, a formula for estimating the exit velocity, U_e, is needed. For elongated patches, U_e/U_∞ depends on $C_d aL$ for $C_d aL < 8$, $L < L_I$, while it becomes constant for $C_d aL > 8$ or $L > L_I$. The measured values of U_e/U_∞ from this study and the studies of Nepf[23], Li et al.[24] and Creed et al.[25] are plotted together to show the variation tendency of U_e/U_∞ (Fig. 6). For a low flow blockage ($C_d aL \le 8$), U_e/U_∞ decreases approximately linearly with increasing $C_d aL$. The best-fit linear function between U_e/U_∞, $C_d aL$ is as follows:

$$\frac{U_e}{U_\infty} = 1 - (0.22\pm0.10)C_d aL \tag{3}$$

When the patch length is smaller than the interior flow adjustment distance ($L < L_I$), the exit velocity decreases as the patch length increases (see Fig. 4(a)), where the interior flow adjustment length (L_I) is

calculated by Eq. (1). When $L > L_I$, the exit velocity is constant. Based on this fact, Eq. (3) is valid only when $L < L_I$. In Fig. 6, the data from Nepf[23], Li et al.[24] and Creed et al.[25] are collected in a channel with a patch-channel ratio b/B between 0.1, 0.2. Equation (3) is valid for $b/B = 0.1\text{-}0.2$. Beyond those ranges, further verification is needed.

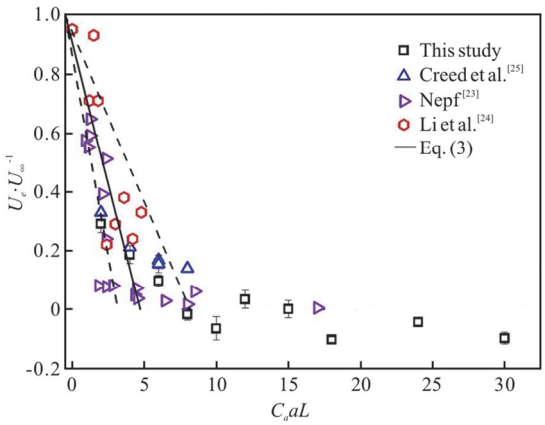

Fig. 6 (Color online) Exit velocity, U_e, normalized by the channel average velocity, U_∞ against the nondimensional parameter, C_daL, based on the experimental data from this study, Nepf[23], Li et al.[24] and the numerical simulation from Creed et al.[25]. The black line is the best-fit line of Eq. (3) with 95% confidential intervals (dashed lines)

Combining Eqs. (2), (3), for $C_daL \le 8$, the length of the wake region, L_w, behind a patch shorter than L_I is predicted as

$$\frac{L_w}{b} = (2.5 \pm 0.5)\left(\frac{9 - C_daL}{C_daL}\right) \tag{4}$$

For a high flow blockage $(C_daL > 8)$, the recirculating flow behind the patches has a similar wake structure as that behind solid bodies[14, 18]. An experimental study (e.g., see Table 1 in Zong and Nepf[14]) and a numerical simulation (see Fig. 10 in Nicolle and Eames[18]) show that the wake region length behind a solid body is $L_w \approx 0$. Note that Eq. (4) suggests that $L_w/b = 0$ for $C_daL = 9$, which is consistent with the limit of $L_w/b\,(=0)$ behind a solid body $(C_daL = +\infty)$. In this study, when $C_daL > 8$, $L > L_I$, the mean of the measurements in three cases (A5, B5 and B6) is also consistent with the published data, shown as

$$\frac{L_w}{b} = 0.3 \pm 0.3 \tag{5}$$

In the cases of $C_daL > 8$, $L > L_I$, the flow inside the patch is fully developed. A further increase of the patch length does not influence the wake region length, and the constant wake region can be estimated by Eq. (5). The measurements agree well with the predictions within the uncertainty margin (Fig. 5(b)). The mean difference between the measurements and the predictions is $MD\left(=1/m\sum_{i=1}^{m}(|M_{\text{mea}} - M_{\text{pre}}|)/M_{\text{mea}}\right) = 12\%$, where m is the number of cases, M_{mea} and M_{pre} are the measurements and the predictions, respectively. This indicates that Eqs. (4), (5) are capable of predicting the wake region length.

2.2 *Turbulent kinetic energy (TKE)*

Figure 7 shows the longitudinal distribution of the TKE behind the patches of two densities (a = 10 m^{-1}, 30 m^{-1}) and three patch lengths ($L = b$, $3b$ and $5b$). First, the local peak of the TKE is observed directly behind the patches with $L/b = 1.0$ (case A1), 3.0 (case A2) for $a = 10$ m^{-1} (denoted by green circles in Fig. 7(a)), which is due to the stem-generated turbulence. Liu and Nepf[9] reported that the threshold in the presence of the stem-generated turbulence behind rigid cylinders is $Re_{d(c)} = 120$. That is, at the patch trailing edge, the stem-generated turbulence occurs when $Re_d\,(=U_ed/\nu) > 120$, while the shut-off occurs when $Re_d < 120$. In cases A1, A2, $U_e = 0.024$ m/s - 0.037 m/s, corresponding to Re_d = 192 - 296 (> 120), which confirms the turbulence generated by individual stems. However, in other cases, $U_e \le 0.013$ m/s, yielding $Re_d \le 104$, all of which are smaller than the threshold $(Re_{d(c)} = 120)$, indicating the absence of the stem-generated turbulence, as consistent with the measurements. No local peak is observed directly behind the patches in all cases apart from A1, A2.

Second, the maximum TKE is observed at a distance $(x = L_{\text{TKE}})$ from the trailing edge of the patches, which is due to the von Karman vortex street (i.e., the patch-generated turbulence) (Fig. 7). The Karman vortices could produce a distinct local peak (e.g., $L/b = 5$ (blue triangles) in Fig. 7(a)), but the vortices might be absent for the shortest patch (e.g., $L/b = 1$ (black squares)) because the local peak is not clear. The presence or absence of the Karman vortices is confirmed by the flow visualization (see Section 2.3).

The intensity of the TKE_{peak} is related to the shear strength behind the patch, and the shear strength

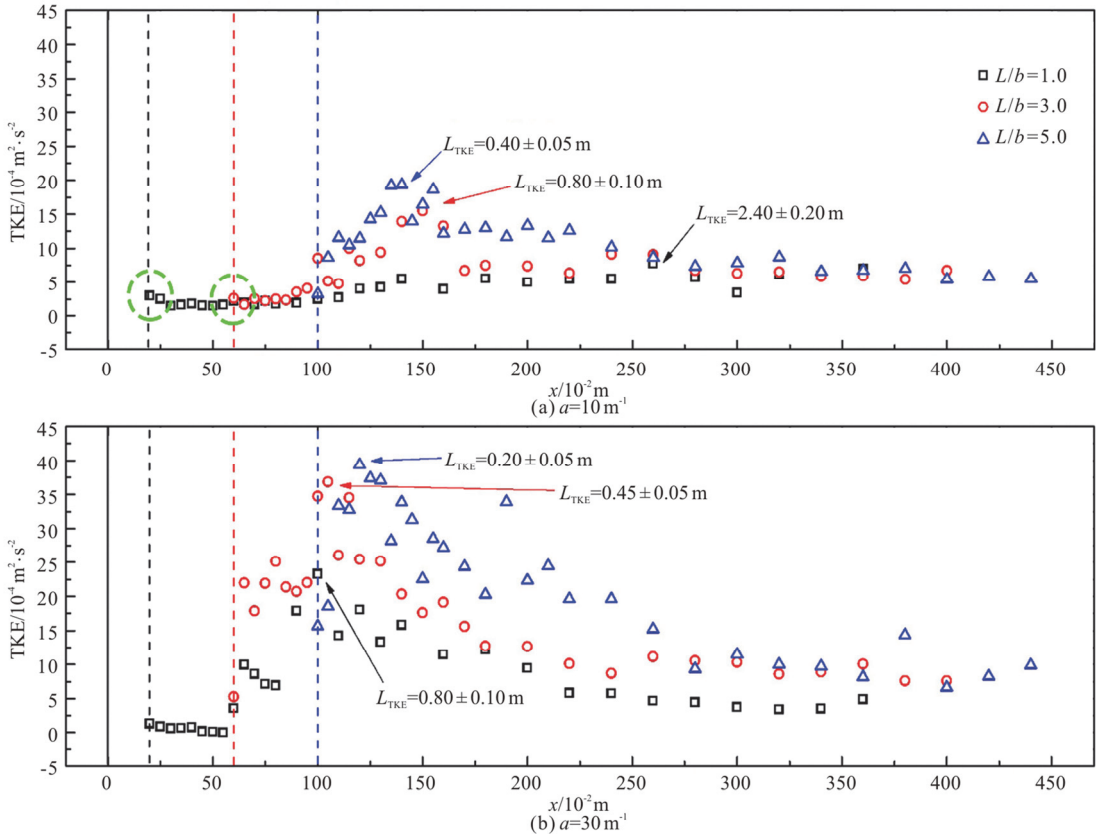

Fig. 7 (Color online) Longitudinal evolution of the turbulent kinetic energy (TKE) behind patches of two densities. The location of the maximum TKE in each case, L_{TKE}, is indicated by the arrow lines. The green circles indicate the stem-generated turbulence

is related to the velocity difference, $(U_2-U_1)^2$, where U_1 and U_2 are the mean velocities in the wake and the bare channel at L_w, respectively (Fig. 1). Recall that the wake flows are related to C_daL and not to C_dab, thus, the velocity in the wake, U_1, normalized by the channel average velocity, U_∞ has a clear dependence on C_daL when $C_daL<8$. When $C_daL>8$, U_1/U_∞ becomes constant (Fig. 8). When $C_daL<8$, the normalized velocity difference, $(U_2-U_1)/U_\infty$, increases as C_daL increases, and when $C_daL>8$, $(U_2-U_1)/U_\infty$ becomes constant (≈ 1.3, Fig. 9(a)). Correspondingly, the maximum turbulence, $\mathrm{TKE}_{\mathrm{peak}}$, in the wake, normalized by $(U_2-U_1)^2$ gradually increases when $C_daL<8$ and becomes constant when $C_daL\geq 12$ (Fig. 9(b)). The constant $\mathrm{TKE}_{\mathrm{peak}}/(U_2-U_1)^2 (=0.19\pm0.04)$ is equal to that $(\approx 0.23\pm0.03)$ behind a solid body within the uncertainty margin (see Fig. 13 in Zong and Nepf[14]), suggesting that the Karman vortices behind the porous patches of $C_daL\geq 12$ are similar to those behind solid bodies.

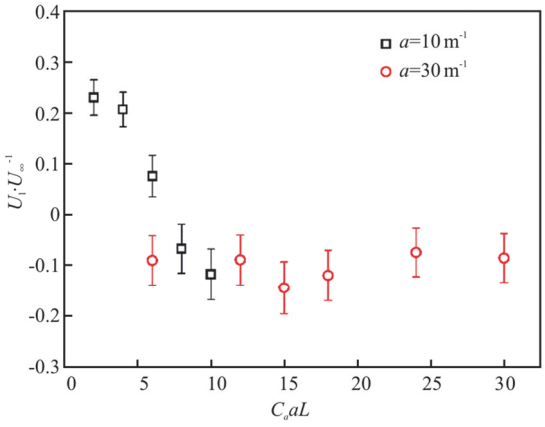

Fig. 8 (Color online) Velocity behind the patch at $x=L_{\mathrm{TKE}}$, U_1, normalized by the channel average velocity, U_∞, against the nondimensional parameter, C_daL

The length scales L_{TKE}, L_w are related when $C_daL<30$, where L_{TKE}, L_w represent the distance from the patch trailing edge to the beginning of the von Karman vortex street and its peak intensity,

respectively. $L_{\mathrm{TKE}} / L_w \approx 4 \pm 2$, suggesting that when the Karman vortices are delayed downstream the patch (a larger L_w), the flow develops more slowly (with a larger L_{TKE}). When the shear strength behind the patches is sufficiently strong to produce the Karman vortices, a shorter and sparser patch (with a smaller $C_d aL$) will produce weaker Karman vortices (with a smaller $\mathrm{TKE}_{\mathrm{peak}} / (U_2 - U_1)^2$).

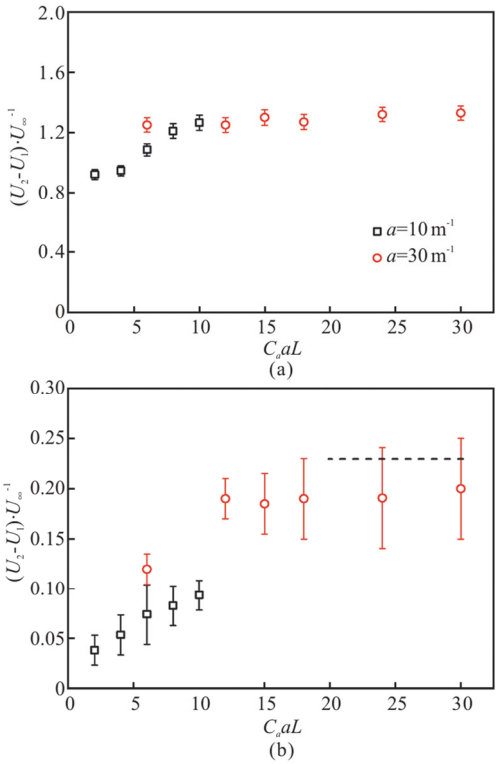

Fig. 9 (Color online) (a) $(U_2 - U_1)/U_\infty$ versus the nondimensional parameter $C_d aL$, which indicates the flow blockage of a patch in the longitudinal direction. (b) The maximum *TKE*, normalized by the velocity difference, $U_2 - U_1$, against $C_d aL$. The mean of $\mathrm{TKE}_{\mathrm{peak}} / (U_2 - U_1)^2 (= 0.19 \pm 0.04)$ for $C_d aL \geq 12$ is the same as that ($\approx 0.23 \pm 0.03$, obtained by Zong and Nepf[14] and denoted by the dashed line) for a solid body

2.3 *Flow visualization*

The length of the steady wake region $(L_{w(\mathrm{dye})})$, determined by the tracer experiments, is compared to those determined by the velocity measurements, L_w (Fig. 10). $L_{w(\mathrm{dye})}$ is in good agreement with L_w, and the difference between $L_{w(\mathrm{dye})}$, L_w is 15% on average, indicating that the tracer experiment could quite accurately determine the length of the steady wake region.

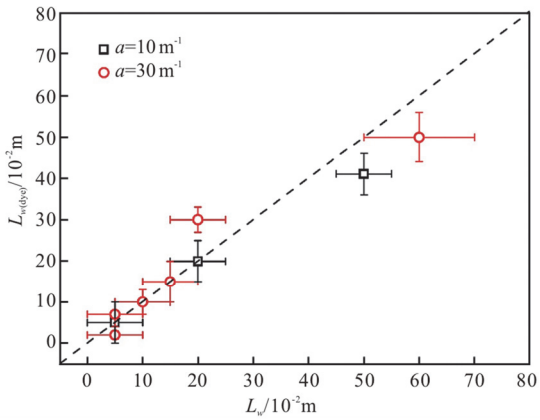

Fig. 10 (Color online) Comparison between the wake length determined by flow visualization $(L_{w(\mathrm{dye})})$ and that determined by velocity measurements (L_w). The dashed line denotes the relation $L_{w(\mathrm{dye})} = L_w$

Next, we discuss the wake structure behind the elongated patches. The visualization shows a similar wake structure as that obtained with the velocity measurements. For the sparse patches $(a = 10\ \mathrm{m}^{-1})$, the longest steady wake region is observed behind the shortest patch ($L = b$ in the case of A1, Fig. 11(a)). The steady wake region becomes shorter as the patch length increases (Figs. 11(b)-11(d)). The shortest steady wake is observed behind the longest patch (case A5, Fig. 11(e)).

The von Karman vortex street is not observed behind the patches of $L = b$, $2b$ (Figs. 11(a), 11(b)). However, the vortex street is observed behind the patches of $L = 3b$-$5b$ (denoted by red arrows, Figs. 11(c)-11(e)), and the vortex street is closer to the patch trailing edge as the patch length increases. When the von Karman vortex street occurs, the lateral oscillation of the Karman vortices was observed at a frequency $f \approx 0.1$ Hz [10, 14-15]. Based on this fact, the velocity spectrum is employed to further confirm the presence of the Karman vortices. No local peak is observed behind the patches of $L = b$, $2b$ (Figs. 12(a), 12(b)), suggesting that the Karman vortices are absent behind the two patches, corresponding to the condition $U_1 / U_\infty > 0.2$ (Fig. 8). In contrast, a local peak is observed for $f = 0.07$ Hz - 0.10 Hz behind the patches of $L = 3b$-$5b$ (Figs. 12(c)-12(e)), indicating that the Karman vortices are present behind the three patches. For dense patches $(a = 30\ \mathrm{m}^{-1})$, when the patch length is the same, the steady wake regions are shorter than those behind sparse patches (Fig. 13). The peak of the velocity spectrum is observed for $f = 0.06$ Hz - 0.11 Hz, suggesting that

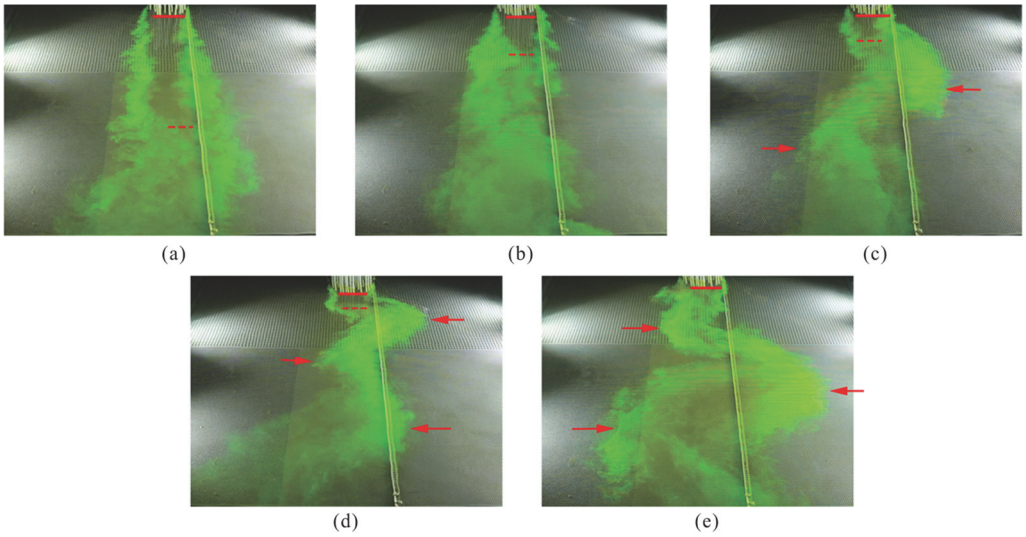

Fig. 11 (Color online) The length of the wake region, $L_{w(\mathrm{dye})}$, behind the model patches in cases A1 through A5 $(a = 10\ \mathrm{m}^{-1})$, based on flow visualization. The five patches have different lengths: (a) Case A1, $L/b = 1.0$, $L_{w(\mathrm{dye})} = 0.92 \pm 0.13$ m. (b) Case A2, $L/b = 2.0$, $L_{w(\mathrm{dye})} = 0.75 \pm 0.12$ m. (c) Case A3, $L/b = 3.0$, $L_{w(\mathrm{dye})} = 0.41 \pm 0.05$ m. (d) Case A4, $L/b = 4.0$, $L_{w(\mathrm{dye})} = 0.20 \pm 0.05$ m. (e) Case A5, $L/b = 5.0$, $L_{w(\mathrm{dye})} = 0.08 \pm 0.05$ m. The flow is from top to bottom in each image. The five images are taken at the instant from different 40-s videos. The periodic lateral excursion can be observed in subplots (c), (d) and (e). The solid red line indicates the patch trailing edge, while the dashed red line indicates the downstream edge of the wake region. The length of the wake region, $L_{w(\mathrm{dye})}$, is the distance between two red lines. In subplots (c)-(e), the Karman vortices are denoted by red arrow lines

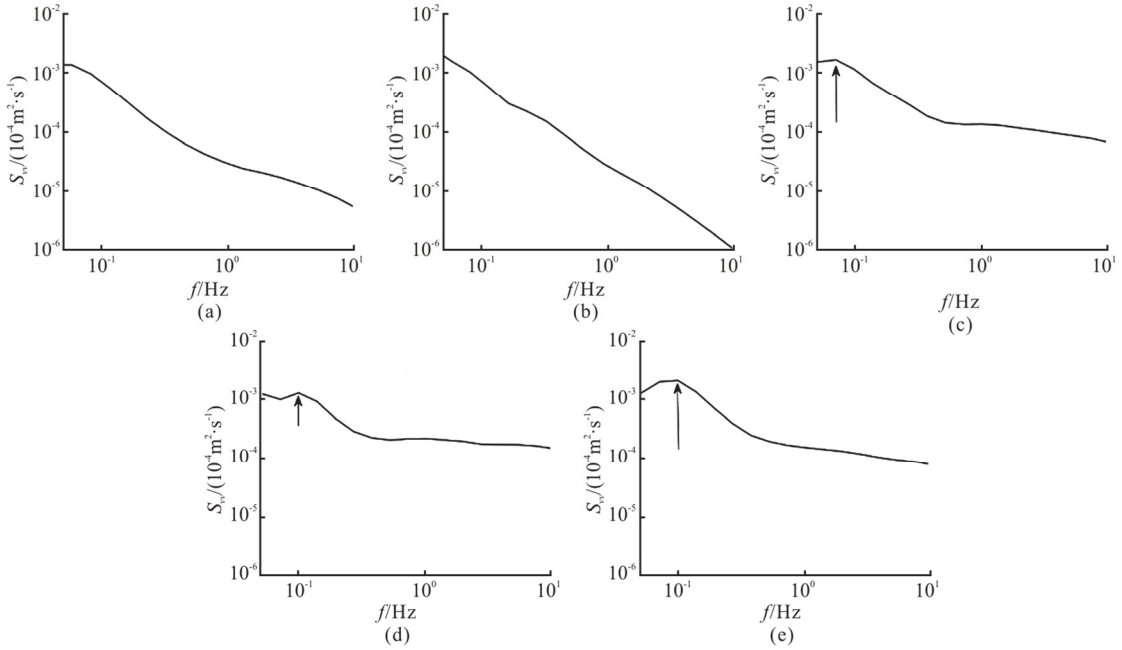

Fig. 12 Velocity spectrum S_{vv} behind sparse vegetation patches of $a = 10\ \mathrm{m}^{-1}$. (a) $L/b = 1.0$ (case A1). (b) $L/b = 2.0$ (case A2). (c) $L/b = 3.0$ (case A3). (d) $L/b = 4.0$ (case A4). (e) $L/b = 5.0$ (case A5). The velocity measured at $x = L_{\mathrm{TKE}}$ is used to obtain S_{vv}. The local peak of the power spectra varies between $f = 0.07$ Hz, 0.10 Hz in subplots (c) through (e), as denoted by the arrows

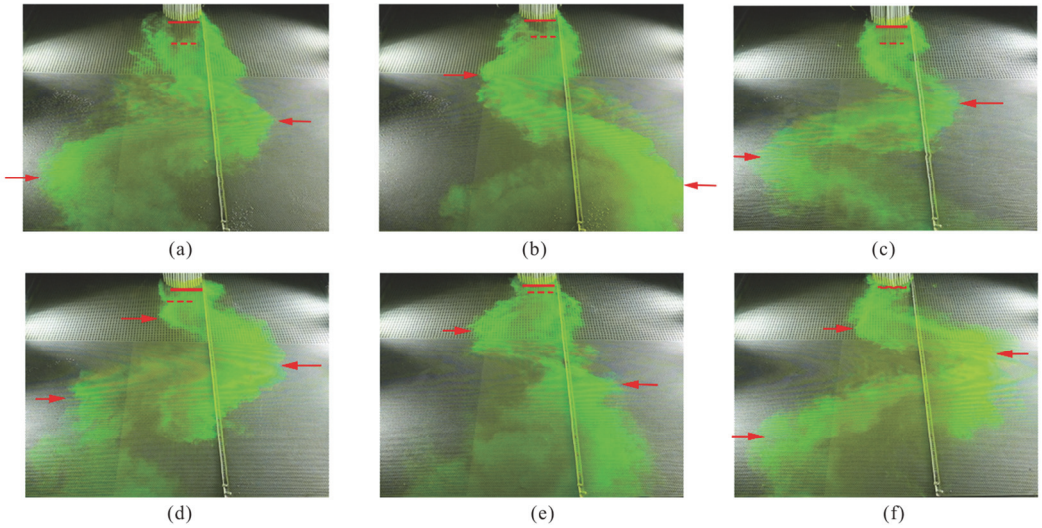

Fig. 13 (Color online) The length of the wake region, $L_{w(\mathrm{dye})}$, behind the model patches in cases B1 through B6 $(a = 30\ \mathrm{m}^{-1})$, based on flow visualization. The six patches have different lengths: (a) Case B1, $L/b = 1.0$, $L_{w(\mathrm{dye})} = 0.50 \pm 0.06$ m. (b) Case B2, $L/b = 2.0$, $L_{w(\mathrm{dye})} = 0.30 \pm 0.03$ m. (c) Case B3, $L/b = 2.5$, $L_{w(\mathrm{dye})} = 0.15 \pm 0.05$ m. (d) Case B4, $L/b = 3.0$, $L_{w(\mathrm{dye})} = 0.10 \pm 0.03$ m. (e) Case B5, $L/b = 4.0$, $L_{w(\mathrm{dye})} = 0.07 \pm 0.03$ m. (f) Case B6, $L/b = 5.0$, $L_{w(\mathrm{dye})} = 0.02 \pm 0.01$ m. The flow is from top to bottom in each image. The six images are taken at the 20th second of 40 s videos. The solid red line indicates the patch trailing edge, while the dashed red line indicates the downstream edge of the wake region. The length of the wake region, $L_{w(\mathrm{dye})}$, is the distance between two red lines. In subplots (a)-(f), the Karman vortices are denoted by the red arrow lines

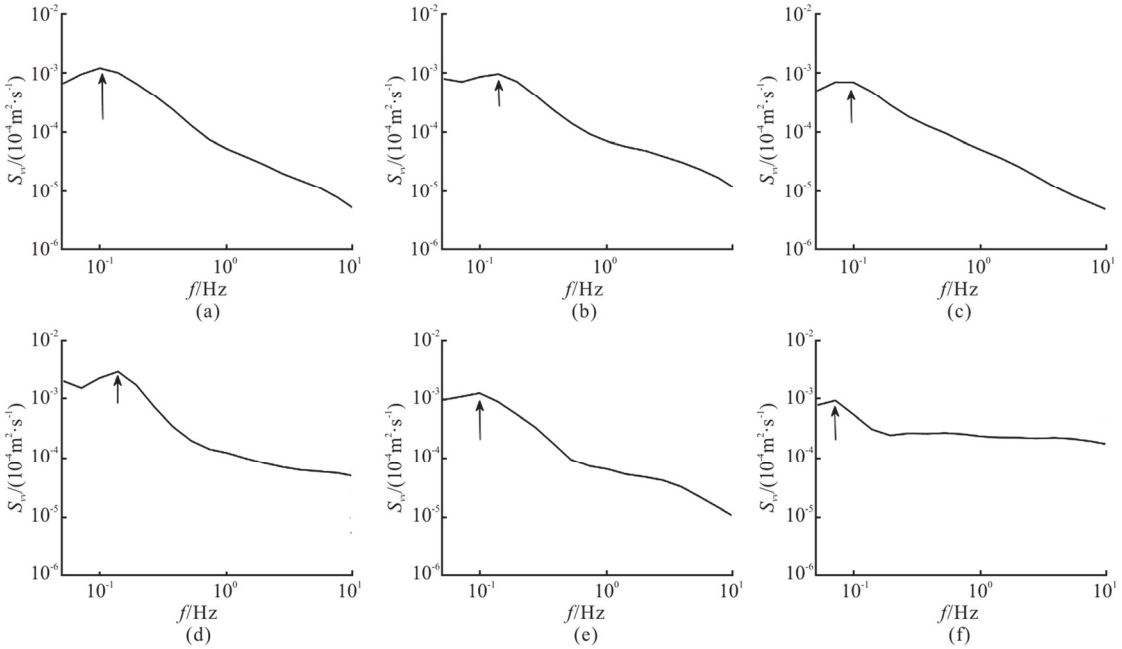

Fig. 14 Velocity spectrum S_{vv} behind sparse vegetation patches of $a = 30\ \mathrm{m}^{-1}$. (a) $L/b = 1.0$ (case B1). (b) $L/b = 2.0$ (case B2). (c) $L/b = 2.5$ (case B3). (d) $L/b = 3.0$ (case B4). (e) $L/b = 4.0$ (case B5). (f) $L/b = 5.0$ (case B6). The velocity measured at $x = L_{\mathrm{TKE}}$ is used to obtain S_{vv}. The local peak of the power spectra varies between $f = 0.06$ Hz, 0.11 Hz in subplots a through (f), as denoted by the arrows

the Karman vortices occur behind all six patches (Fig. 14).

3. Discussions

The experimental results can be used to explain the expansion pattern of a vegetation patch in the streamwise direction from a hydrodynamic viewpoint.

The steady wake region of an emergent elongated patch diminishes with the increase of $C_d aL$ and reaches its minimum size when $C_d aL \geq 8$ (Section 2.1). Therefore, $C_d aL = 8$ can be considered as the critical condition for the steady wake region of an elongated patch to reach its minimum size. The critical patch length for reaching the minimum length of the steady wake region can be estimated from the relation $L_c = 8 / C_d a$. When the patch length L is shorter than L_c, the patch wake does not reach its minimum size, and a net deposition in the patch wake should be observed. For example, Bouma et al.[6] constructed model patches $(a = 0.2\ \mathrm{m}^{-1} - 2.8\ \mathrm{m}^{-1})$ in inertial regions using rigid stems. The patch length $L (= 2.0\ \mathrm{m})$ was smaller than the critical patch length L_c (=2.9 m, 45.0 m for dense and sparse canopies, respectively), hence, an enhanced deposition was observed directly behind the patches (see Fig. 3(a) in Bouma et al.[6]). Similarly, Follett and Nepf[11] constructed model patches $(a = 6\ \mathrm{m}^{-1} - 20\ \mathrm{m}^{-1})$ with lengths $L = 0.10\ \mathrm{m} - 0.22\ \mathrm{m}$ that were smaller than $L_c\ (= 0.40\ \mathrm{m} - 1.33\ \mathrm{m})$, thus, a net deposition occurred directly behind those patches. Given the above observations, the net deposition in a patch wake will occur when $L < L_c$, which should promote the vegetation growth in the longitudinal direction. If the condition is appropriate for the vegetation growth, the patch length, L, could continue to increase until L reaches the critical patch length, L_c.

When the steady wake region reaches its minimum size, the Karman vortices occur almost directly behind the patch. The wake structure of the porous patches is similar to that of the solid bodies; thus, the net deposition will not occur in the patch wake. Instead, the bed erosion is expected to occur behind the patches, similar to that behind a solid body[26]. Chen et al.[16] investigated the channel bed scours around model patches. In their study, a model patch of $a = 65\ \mathrm{m}^{-1}$ was constructed, and the patch length $L (= 0.15\ \mathrm{m})$ was greater than $L_c\ (= 0.12\ \mathrm{m})$, indicating that the patch was sufficiently long for the steady wake region to reach its minimum size. As expected, the bed erosion was observed directly behind the patch (see Fig. 12 in Chen et al.[27]). The erosion of the channel bed behind a patch will prevent the patch from extending in the longitudinal direction; thus, the patch length will not increase.

The above discussion can further explain the patch length commonly observed in the field. In natural rivers and wetlands, the vegetation density is $a = 1.2\ \mathrm{m}^{-1} - 35\ \mathrm{m}^{-1}$ for rigid and flexible plants, e.g., *Scripus maritimus*, *Callitriche platycarpa*[28-29], yielding critical patch lengths of $L_c\ (= 8 / C_d a) \approx 0.25\ \mathrm{m} - 6.50\ \mathrm{m}$. The sediment attached with nutrients and organic matter would tend to deposit in the wake to promote the longitudinal patch growth until the patch length reaches the critical length $(L = L_c)$. Based on this observation, the observed length of the patches $L \approx 0.2\ \mathrm{m} - 5.0\ \mathrm{m}$ in the field[1, 2, 30] is mostly in the range of the critical patch length $L_c\ (= 0.25\ \mathrm{m} - 6.50\ \mathrm{m})$. However, we note that in this study, the analysis explains only the longitudinal development of an individual patch. The interaction between the vegetation patches and the spatial distribution of the patches affected by the channelized flows might impact the patch length, which is not the focus of this study.

4. Conclusion

This study investigates the wake flow structure behind model patches of emergent vegetation that are elongated in the streamwise direction. Patches with the same width but different lengths are designed. Behind those patches, the steady wake region length, L_w, is not a function of the width-related flow blockage, $C_d ab$, but a function of the length-related flow blockage, $C_d aL$. Specifically, when $0 < C_d aL < 8$, L_w decreases as $C_d aL$ increases, whereas when $C_d aL > 8$, L_w reaches its minimum and remains constant. A previous model is revised and adapted to predict L_w (Eqs. (4), (5)). The predictions are in good agreement with the measurements. Furthermore, the flow visualization is employed to accurately estimate L_w. In all cases, the difference of the values of L_w determined by the flow visualization and the velocity measurements is 15% on average. A von Karman vortex street occurs behind the patches only if the ratio of the wake flow velocity, U_1, to the velocity in the bare channel, U_∞, is less than 0.2, that is, $U_1 / U_\infty < 0.2$. As the patch becomes longer and/or denser, the Karman vortices occur closer to the patch trailing edge and a stronger turbulence magnitude is produced beyond the steady wake region. When the flow blockage is sufficiently large $(C_d aL > 8)$, the Karman vortices are observed

directly behind the porous patches, similar to those behind the solid bodies. These results can be used to explain the patch elongation in the longitudinal direction. Once a patch extends to the critical patch length, $L_c\ (=8/C_d a)$, in the streamwise direction, the Karman vortices appear directly behind the patch and a further longitudinal extension of the patch is prevented.

Acknowledgments

This work was supported by the Sichuan Science and Technology Program (Grant No. 2021YFH0028), the China Scholarship Council (Grant No. 202006240062).

References

[1] Sand-Jensen K., Pedersen Morten L. Streamlining of plant patches in streams [J]. *Freshwater Biology*, 2008, 53(4):714-726.

[2] Cornacchia L., van de Koppel J. Landscapes of facilitation: How self-organized patchiness of aquatic macrophytes promotes diversity in streams [J]. *Ecology*, 2018, 99(4): 832-847.

[3] Liu C., Shan Y. Analytical model for predicting the longitudinal profiles of velocities in a channel with a model vegetation patch [J]. *Journal of Hydrology*, 2019, 576: 561-574.

[4] Liu C., Shan Y., Nepf H. Impact of stem size on turbulence and sediment resuspension under unidirectional flow [J]. *Water Resources Research*, 2021, 57(3): e2020WR028620.

[5] Elsey-Quirk T., Graham S. A., Mendelssohn I. A. et al. Mississippi river sediment diversions and coastal wetland sustainability: Synthesis of responses to freshwater, sediment, and nutrient inputs [J]. *Estuarine, Coastal and Shelf Science*, 2019, 221: 170-183.

[6] Bouma T. J., van Duren L. A., Temmerman S. et al. Spatial flow and sedimentation patterns within patches of epibenthic structures: Combining field, flume and modelling experiments [J]. *Continental Shelf Research*, 2007, 27(8): 1020-1045.

[7] Przyborowski Ł., Łoboda A. M. Identification of coherent structures downstream of patches of aquatic vegetation in a natural environment [J]. *Journal of Hydrology*, 2021, 596: 126123.

[8] Yu Z., Wang D., Liu X. Impact of vegetation density on the wake structure [J]. *Water*, 2019, 11(6): 1266.

[9] Liu C., Nepf H. Sediment deposition within and around a finite patch of model vegetation over a range of channel velocity [J]. *Water Resources Research*, 2016, 52(1): 600-612.

[10] Hu Z., Lei J., Liu C. et al. Wake structure and sediment deposition behind models of submerged vegetation with and without flexible leaves [J]. *Advances in Water Resources*, 2018, 118: 28-38.

[11] Follett Elizabeth M., Nepf H. M. Sediment patterns near a model patch of reedy emergent vegetation [J]. *Geomorphology*, 2012, 179: 141-151.

[12] Huai W. X., Zhang J., Katul Gabriel G. et al. The structure of turbulent flow through submerged flexible vegetation [J]. *Journal of Hydrodynamics*, 2019, 31(2): 274-292.

[13] Liu X., Zeng Y., Huai W. Modeling of interactions between floating particles and emergent stems in slow open channel flow [J]. *Water Resources Research*, 2018, 54(9): 7061-7075.

[14] Zong L., Nepf H. Vortex development behind a finite porous obstruction in a channel [J]. *Journal of Fluid Mechanics*, 2012, 691: 368-391.

[15] Liu C., Hu Z., Lei J. et al. Vortex structure and sediment deposition in the wake behind a finite patch of model submerged vegetation [J]. *Journal of Hydraulic Engineering, ASCE*, 2018, 144(2): 4017065.

[16] Chen Z., Ortiz Alejandra, Zong L. et al. The wake structure behind a porous obstruction and its implications for deposition near a finite patch of emergent vegetation [J]. *Water Resources Research*, 2012, 48(9): W09517.

[17] Shan Y., Zhao T., Liu C. et al. Turbulence and bed load transport in channels with randomly distributed emergent patches of model vegetation [J]. *Geophysical Research Letters*, 2020, 47(12): e2020GL087055.

[18] Nicolle A., Eames I. Numerical study of flow through and around a circular array of cylinders [J]. *Journal of Fluid Mechanics*, 2011, 679: 1-31.

[19] Yan C., Shan Y., Sun W. et al. Modeling the longitudinal profiles of streamwise velocity in an open channel with a model patch of vegetation [J]. *Environmental Fluid Mechanics*, 2020, 20(8): 1441-1462.

[20] Liu C., Shan Y., Sun W. et al. An open channel with an emergent vegetation patch: Predicting the longitudinal profiles of velocities based on exponential decay [J]. *Journal of Hydrology*, 2020, 582: 124429.

[21] Schoelynck J., de Groote T., Bal K. et al. Self-organised patchiness and scale-dependent bio-geomorphic feedbacks in aquatic river vegetation [J]. *Ecography*, 2012, 35(8): 760-768.

[22] Goring D. G., Nikora V. I. Despiking acoustic Doppler velocimeter data [J]. *Journal of Hydraulic Engineering, ASCE*, 2002, 128(1): 117-126.

[23] Nepf H. M. Hydrodynamics of vegetated channels [J]. *Journal of Hydraulic Research*, 2012, 50(3): 262-279.

[24] Li W. Q., Wang D., Jiao J. L. et al. Effects of vegetation patch density on flow velocity characteristics in an open channel [J]. *Journal of Hydrodynamics*, 2019, 31(5): 1052-1059.

[25] Creed M. J., Draper S., Nishino T. et al. Flow through a very porous obstacle in a shallow channel [J]. *Proceedings of the Royal Society A-Mathematical Physical and Engineering Sciences*, 2017, 473(2200): 20160672.

[26] Neary V. S., Constantinescu S. G., Bennett S. J. et al. Effects of vegetation on turbulence, sediment transport, and stream morphology [J]. *Journal of Hydraulic Engineering, ASCE*, 2012, 138(9): 765-776.

[27] Chen S. C., Kuo Y. M., Yen H. C. Effects of submerged flexible vegetation and solid structure bars on channel bed scour [J]. *International Journal of Sediment Research*, 2012, 27(3): 323-336.

[28] Schoelynck J., Meire D., Bal K. et al. Submerged macrophytes avoiding a negative feedback in reaction to hydrodynamic stress [J]. *Limnologica*, 2013, 43(5): 371-380.

[29] Jahadi M., Afzalimehr H., Rowinski P. M. Flow structure within a vegetation patch in a gravel-bed river [J]. *Journal of Hydrology and Hydromechanics*, 2019, 67(2): 154-162.

[30] Licci S., Nepf H., Delolme C. et al. The role of patch size in ecosystem engineering capacity: a case study of aquatic vegetation [J]. *Aquatic Sciences*, 2019, 81(3): 41.